CHAPTER 5

SMARTPHONE PLATFORM PHOTOMETRIC AND FLUORESCENCE SENSING FOR TRACE DETECTION OF NITRITE IN SOIL AND WATER

Present chapter discusses the importance of monitoring of nitrite level and the realization of alternative smartphone based sensing system using commonly used optical components. The goal of the present work is to develop a dual mode sensing system using a smartphone by which nitrite level in different media can be estimated reliably. The sensing principle is based on both photometric and fluorescence intensities variation of carbon nanodot (C-dot) and neutral red (NR) mixture that occurs that occurs due to frequency resonance energy transfer (FRET) process in presence of nitrite level in the medium. The utilization of inbuilt sensors of the phone for development of dual mode sensing system and android applications for data acquisition and analysis within the device have been demonstrated. The designed sensor has been implemented to estimate the nitrite level of infield water and soil samples, and the experimental results were compared with the laboratory standard tools. At the end of the chapter, the advantages and feasibility of the proposed smartphone sensor as a potential avenue for onsite assessment of other parameters of water and soil have been discussed.

5.1 Introduction

Nitrite NO_2^- is widely utilized as a food color and preservative due to its antibacterial property [1, 2]. In addition, it is routinely employed as a coloring substitute, anti-corrosion agent, and chemical fertilizer [3, 4]. Again, due to the agricultural runoff and waste discharge from dying and pharmaceutical industries nitrite has become a

major pollutant for surface and groundwater resources [5, 6]. The excess content of nitrite in water and soil is harmful to human health and could cause pollutions to the water resources, which may lead to the extinction of some aquatic lives. Nitrite reacts with secondary and tertiary amines to form carcinogenic N-nitrosoamines, leading to cancer and hypertension in humans [7]. An excess amount of nitrite in the body may cause an irreversible interaction with haemoglobin, resulting in methemoglobin in the blood, which is the cause of "blue baby syndrome" that is extremely harmful to babies and pregnant women [8, 9]. Thus, monitoring nitrite in water, food and other environmental sources is very important as far as human health is concerned. The acceptable limit of nitrite in drinking water as set by the World Health Organization (WHO) and the United States Environmental Protection Agency (USEPA) is 3.0 mg/L and 1.0 mg/L (as nitrite nitrogen), respectively [2, 10, 11]. Considering its impact on our health and environment, it is needed to develop a suitable sensing platform that can detect the nitrite level concentrations in water and soil at the point of care level. Although, different techniques exist to detect nitrite level in various media such as spectrophotometry [12, 13], electrochemical [14–17], chromatography [18–20], molecular absorption spectrometry [21, 22], Raman spectrometry [23, 24], chemiluminescence [25, 26] etc. However, all these techniques demand bulky and expensive equipment, a standard laboratory environment, and technical knowledge to operate these tools.

A smartphone is capable of fulfilling all the requirements for the development of a sensing system which has an ability to detect, analysis, and data transfer from the remote location to the central laboratory. The key to the successful implementation of smartphone-based sensing is the advanced hardware and software parts, along with the various sensors embedded within the phone itself. In the present work, standard Griess-based colorimetric method has been used to estimate the nitrite level in soil and water using the smartphone. Puangpila et al. reported mobile phone-based nitrite sensing using the standard Griess-based colorimetric method [27]. As this method is color dependent, it may affect the experimental results due to the presence of other chemicals in the medium. Moreover, this method is not very sensitive to detect trace levels of nitrite in the sample. Owing to its high sensitivity, and relatively low-cost techniques, the fluorescence-based sensing technique has been recently deployed to monitor water quality [28–30]. Fluorescent signal emission from carbon quantum dots (CQDs) has drawn significant interest due to its strong fluorescence properties, and relatively easier to synthesis, low toxicity with very good optical and chemical stability [31–33].Very recently, Carbon nanodots based fluorescence resonance energy transfer (FRET) has been successfully applied for chemical sensing [34], bio-imaging and bio-sensing studies [35]. Wang et al. [36] have reported the colorimetric detection of NO_2^- using polymer-carbon nanodots (PCNDs) on a smartphone. The group has

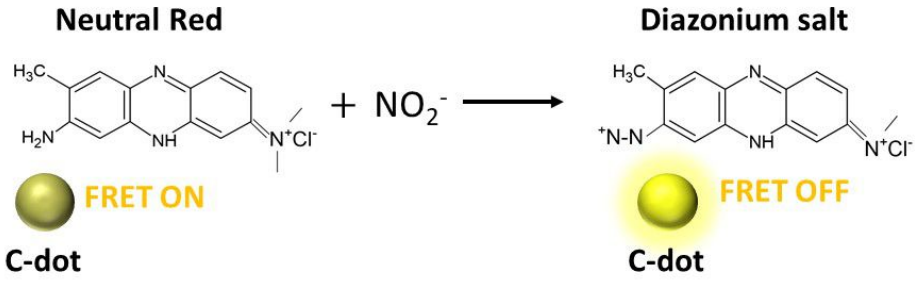

Figure 5.1: Illustration of the mechanism of nitrite in the C-dot-NR medium.

used ΔRGB values for quantitative analysis of NO_2^- based on the color intensity of the samples using a background color. However, the intensity of the background color might affect the colorimetric response of the NO_2^- samples. Also, a better sensitivity can be achieved by considering the HSV color model of each parameter. In another report by Zhang et al. [37], the electrokinetic stacking (ES) mechanism has been integrated with the colorimetric Griess reaction-based method for the detection of nitrite using a smartphone . Although a low limit of detection could be achieved; the sensor response was not linear for a wide range (0.075 to 1.0 g/ml). Li et al. [38] have reported a novel ratiometric FRET-based analysis for the visual quantification of nitrite in sausage samples. The reported synthesis process of quantum dots (QDs) involved several steps compared to the present synthesis procedure of C-dots.

The present work demonstrates the development of a compact smartphone-based sensing platform for dual detection of trace level of nitrite using C-dot and NR. In this work, the C-dot-NR mixture shows the FRET process whose property can be tuned with the presence of nitrite in the mixture. The C-dot-NR mixture exhibits both photometric and fluorescence signals variations with the presence of nitrite in the medium. This dual-mode of response has been used to correlate the concentration of nitrite in the sample. For the C-dot-NR sensing medium, the C-dot acts as a donor while NR acts as an acceptor. The fluorescence emission from the C-dot is quenched by the NR in the mixture via the FRET process. The presence of nitrite in the C-dot-NR medium inhibits the FRET process and thus shows both colorimetric and fluorescence variations with the nitrite level variations in the medium, as shown in figure 5.1. A compact field-portable and user-friendly smartphone sensing system operates both in photometric and fluorescence mode has been designed to monitor these variations. The detailed smartphone-based dual sensing approach of nitrile level has been discussed in the following sections.

5.2 Working principle of the designed smartphone-based sensing system

5.2.1 Design of the photometric sensor on the smartphone

For the photometric mode of sensing, the proposed sensor utilizes the well-known Beer-Lambert's principle. When a beam of light travels throughout a medium, the amplitude of the light signal is attenuated due to the medium's absorption. The absorbance of the propagated light signal depends on the light path length and the proportion of the attenuating medium [39, 40]. The medium's absorbance can be stated as

$$A = \epsilon l c \tag{5.1}$$

where, A is the absorbance of the attenuating medium, which is the ratio between transmitted light intensity and incident light intensity, ϵ is the molar attenuation coefficient, l is the optical path length, and c is the concentration of the attenuating medium. With a specific medium with constant optical path length, the medium's absorbance is directly proportional to its concentration.

5.2.2 Design of the fluorescence mode of sensing for the proposed sensor

The C-dot-NR mixture emits fluorescence signal at the peak wavelength of 563 nm when the medium is irradiated with a UV source. The emitted signal from the sample is allowed to pass through a long-pass optical filter (500 nm) and finally is coupled to the CMOS imaging sensor by using a focusing lens. The CMOS imaging sensor of the phone records the fluorescence signal intensity in the RGB color model, which can be easily converted to HSV color model using simple conversion formula. In the present work, HSV color model's V-channel value has been used to correlate the fluorescence signal intensity with the concentration of the nitrite present in the medium. The variations of the V-channel value in the HSV color model are found to be more sensitive and linear than the H and S-channel variations; thus, provides a better mode of sensing while considering this channel value for nitrite level concentrations in the medium. The V-parameter of the HSV color model represents different shades of the same color [41–43]. So, the change in the V component with the shade of a color can be used for fluorescence-based quantification of an analyte. The V-parameter of HSV color space can be determined from RGB color space from the following equation:

$$V = \frac{\frac{1}{3} \times (R + G + B)}{255} \tag{5.2}$$

where R, G and B represent the red, green and blue channels of RGB color space, respectively. The magnitude of the value component varies from 0 to 1.

5.3 Material and methods

5.3.1 Reagents and Chemicals

All chemicals used in the present study are of research-grade and have been used as received from the suppliers. Polyethylene glycol 200 (PEG 200), sucrose, sodium nitrite ($NaNO_2$), sulfuric acid and hydrochloric acid were procured from Merck, India. Sulfanilamide reagent, N-(1-naphthyl) ethylenediamine dihydrochloride (NED) and neutral red (NR) reagent were procured from Sigma-Aldrich Inc. The deionized (DI) water was used throughout the work, which has been acquired from a Milli-Q water filtering system.

5.3.2 Instrumentation

Images of the synthesized C-dot sample have been acquired using transmission electron microscope (TECNAI G2 20 S-TWIN, FEI Company, USA). All fluorescence signal intensities from the C-dot sample were recorded with a standard fluorescence spectrometer (Hitachi F-7000, Tokyo, Japan). Standard UV-Visible spectrometer (UV 2450, SHIMADZU) was used for photometric analysis. The pH values of the aqueous medium are monitored using a laboratory standard pH metre (Cyber Scan pH 700).

5.3.3 Synthesis of the C-dots

The C-dots have been synthesized using a one-step microwave-assisted synthesis procedure with small modifications [29]. In a 10 mL glass tube, 30% w/v sucrose of volume 1 mL, 200 L concentrated H_2SO_4, and 6 ml PEG is mixed sequentially. The mixed solution is then warmed up in a 700W microwave oven for 20s. The solution gradually turned into golden yellow color, implying the formation of C-dots. Upon cooling, the C-dot solution was centrifuged at a speed of 5000 RPM for 10 minutes in room temperature condition to remove the unsolvable impurities. The volume of the C-dots solution was adjusted to 100 mL by adding distilled water and stored at 4°C for later use.

5.3.4 Optimization of experimental conditions

Different combinations of concentration of C-dot solution, neutral red and pH values of the media have been explored to achieve the optimum experimental condition for the present sensing system. C-dot sample of volume 1 ml has been mixed with different amounts of neutral red (20, 40, 50, 60, 80, 100, 150 and 160 μL) at different pH values (1.0, 1.5, 1.7, 2.0, 3.0, 4.0, and 5.0) with the addition of 1 μg/ml nitrite to analyze the optimal condition. Out of the different combinations, we noticed a mixture of 1 ml C-dot solution, 60 μL of NR and 100 μL of HCl at a pH value of 2.0 yields an optimal sensitivity condition for the designed sensing set-up. 5 minutes of reaction time has been considered to synthesize the proposed reagent, and the prepared sample is then diluted to 5 ml with DI water prior to the spectroscopic analysis.

5.3.5 Fabrication of the designed smartphone-based photometric sensing system

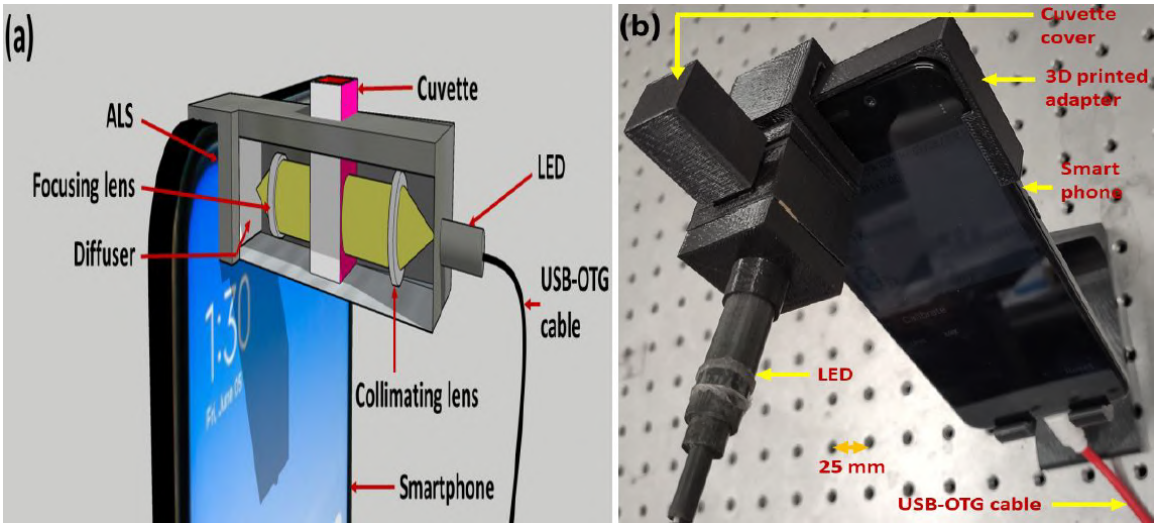

Figure 5.2: (a) Schematic representation (b) photo image of the designed smartphone photometric based sensor.

The schematic diagram of the proposed smartphone-based sensor that operates in photometric sensing mode is shown in figure 5.2(a). An LED with a peak wavelength of 560 nm and full-width half-maximum (FWHM) 10 nm has been utilized as a light source for the current sensing studies. The LED has been powered from the smartphone battery through a USB-OTG cable. The light signal from the LED was allowed to pass through a collimating lens (7 mm diameter, Edmund Optics, product id. 32-404) of focal length 11 mm. The collimated light beam propagates through the C-dot-NR medium placed in a quartz cuvette of optical path length 10 mm. The

modulated light signal via the sample was focused tightly with a focusing lens (6 mm diameter, Edmund Optics), and finally, the transmitted optical signal was coupled to the ambient light sensor (ALS) of the phone (Moto one power). A 1 mm thick glass diffuser (Model no. HO-DF-50S-32, Holmarc optics, India) was used in the optical path to avoid any possible fluctuations of the signal intensities due to the coupling of the intense light signal from the medium. A custom-designed 3D printed optical setup has been fabricated to hold the optical components as well as the sample holder together. The photo image of the designed sensor is shown in figure 5.2(b).

5.3.6 Fabrication of the designed smartphone-based fluorescence sensing system

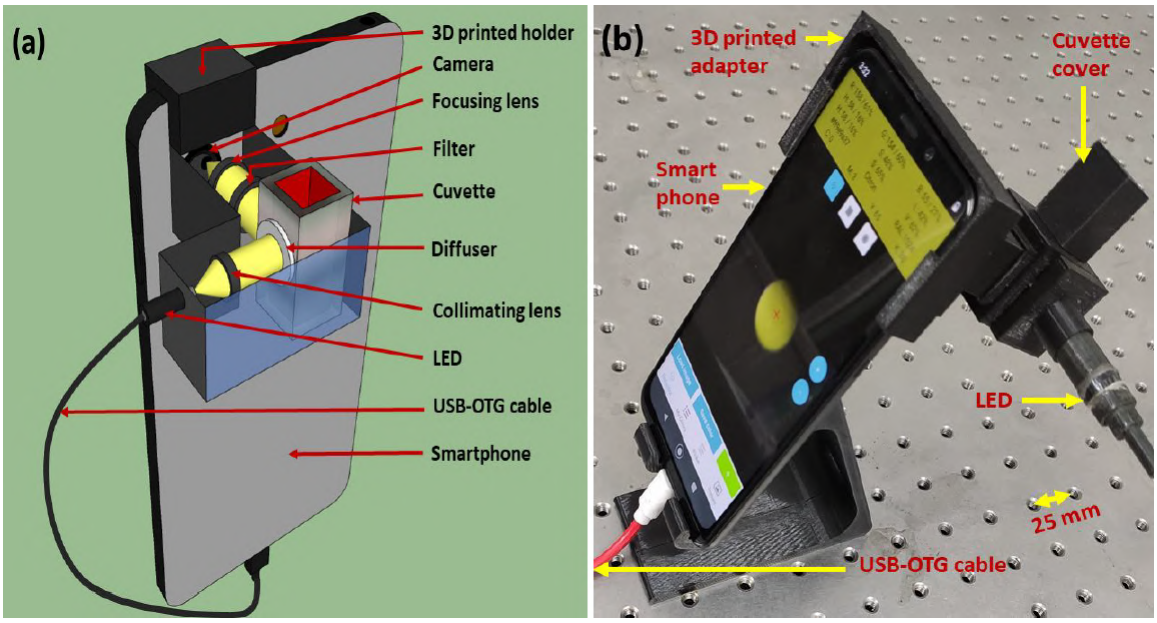

Figure 5.3: (a) Schematic representation (b) captured image of the developed fluorescence sensor.

Figure 5.3(a) illustrates the schematic of the proposed fluorescence-based sensing setup. It consists of a UV LED that emits a light signal with a peak emission wavelength of 375 nm. By using a collimator lens, light signal from this source was made collimated and was allowed to pass through a diffuser so that the beam incident uniformly over the sample. For fluorescence based measurement, the detector is set at 90° angle to the incident light to avoid any interference from the transmitted excitation light. Therefore, the angle of incidence has been considered as 90° to the incident light in order to minimize the fraction of excitation light entering to the detector i.e. the CMOS sensor. To eliminate the excitation wavelength, a 500 nm long-pass optical filter has been placed in the signal's optical path to the imaging sensor of the phone. The fluorescence signal from the sample is focused using a

focusing lens (6 mm diameter, Edmund Optics) and finally coupled to the CMOS imaging sensor (16 MP, 1920 ×1080 pixels) of the phone. Figure 5.3(b) shows the photograph of the designed sensor.

5.3.7 Workflow of the android applications

For photometric mode of sensing, an open-access application available in Android operating system - "Light meter" has been used to calculate the transmitted modulated light intensity from the sample. The application converts the light intensity variations recorded by the ALS of the phone in to "LUX" unit. Light signal intensity transmitted from distilled water has been considered for referencing of the sensing signals. Again, for the fluorescence mode of sensing, another open-access application- "RGB color detector" has been used in the present study. By using this application, the V-parameter value of the captured signal acquired by the phone can be estimated. For analyzing the experimental data for these two modes of sensing, another freely available application- "StanXY" has been used in the present study. By using this application, one can easily obtain the calibration curves for both the modes of sensing with the developed sensor. After attaining the calibrated equations, nitrite level concentration of an unknown medium can be determined by putting the sensing response data in the respective equations.

5.4 Characterization of the synthesized C-dots

5.4.1 Transmission electron microscopes (TEM) imaging

The synthesized C-dots in the present work showed good fluorescence emission. The sucrose and the PEG 200 act as a carbon source and passivation agent, respectively [44]. The structure of the prepared C-dots was examined by transmission electron microscopy (TEM). Figure 5.4(a) displays the TEM image of C-dots, which illustrates a well-dispersed and spherical C-dots of mean diameter of 5.5 nm. The C-dot sample under natural light condition shows light yellow color while upon irradiation with UV light of wavelength 375 nm it emits bright greenish-yellow fluorescence as shown in figures 5.4(b) and 5.4(c), respectively.

This fluorescence emission signal is in accordance with the findings of a previously reported work [45]. The use of C-dot as one of the component of the sensing medium offers several important advantages like low-cost, simple synthesis procedure, and no toxicity. The C-dots can also be synthesized from different ordinary carbon resources like potato, carbohydrate, and candle smoke [46].

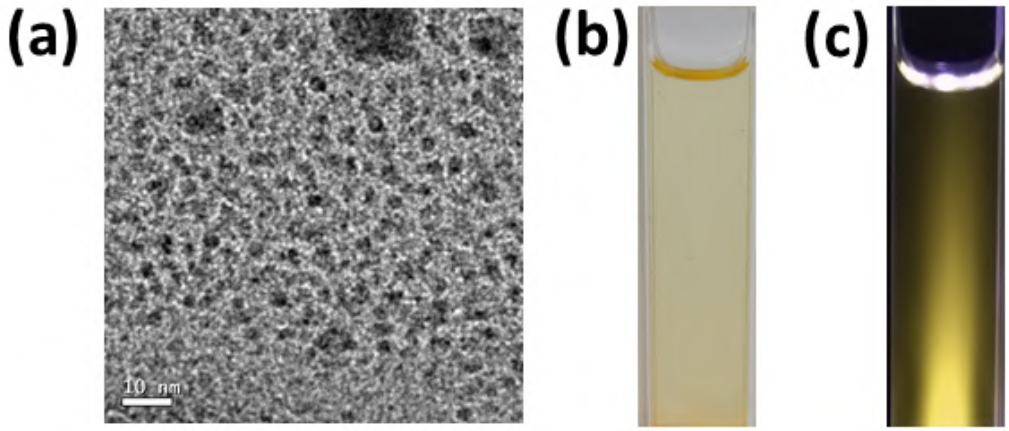

Figure 5.4: (a) TEM image of synthesized C-dots (b) snapshot of the synthesized C-dots under ambient light (c) C-dots fluorescence emission under UV light of wavelength of 375 nm.

5.4.2 Fourier transform infrared (FTIR) spectroscopy analysis

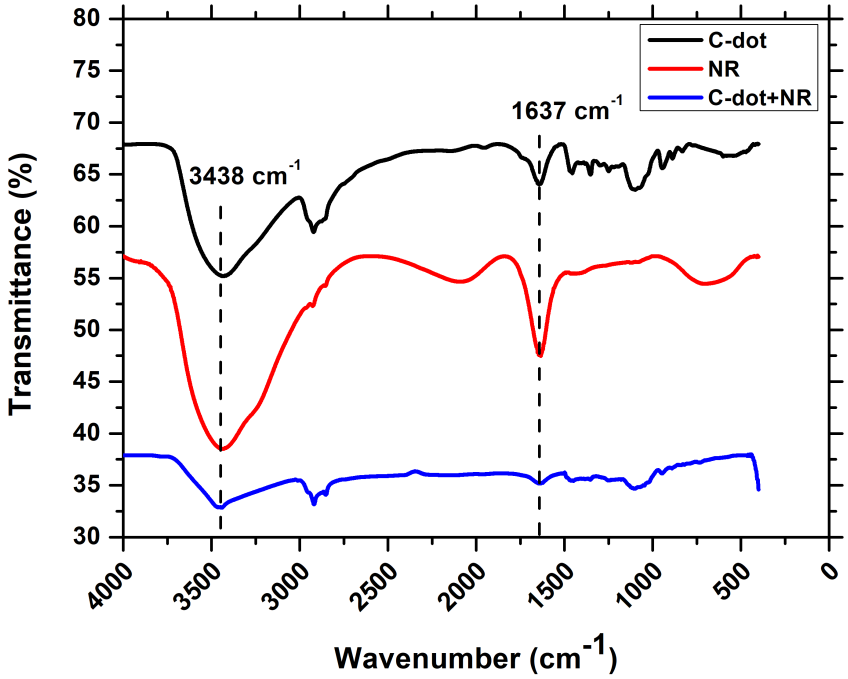

Figure 5.5: FTIR spectra of synthesized C-dot, neutral red and mixed solution of C-dot and neutral red.

Figure 5.5 shows the FTIR spectra of C-dots, NR and the mixture of C-dot-NR. The IR spectrum of the C-Dots and neutral red reveals the two important bands at 3450 cm^1 and 1650 cm^1 assigned to the oxygen-containing groups. The band centered at 3438 cm^1 has resulted from the stretching mode of $-$OH and the band at 1637

cm^1 is derived from the stretching mode of C=O. The decrease in the transmittance of C-dot NR mixed solution indicates the quenching of the fluorescence intensity of C-dot by NR.

5.4.3 Condition and verification of ocuurance of FRET

The UV-Vis spectrum of both C-dot and NR samples have been studied to further confirm the occurrence of the process. Figure 5.6 shows that the peak fluorescent emission wavelength and peak absorption wavelength conditions were at 522 nm and 530 nm, respectively. The absorbance spectra of acceptor- neutral red is almost overlapped with the emission spectra of donor C-dot. For the FRET process to occur, the absorption spectra of the donor should overlap the emission spectra of the acceptor fluorophore, and the distance between the two molecules should be in close proximity [47]. Clearly, the overlapping spectra in figure 5.6 indicates the occurrence of the FRET between the donor C-dot and the acceptor NR.

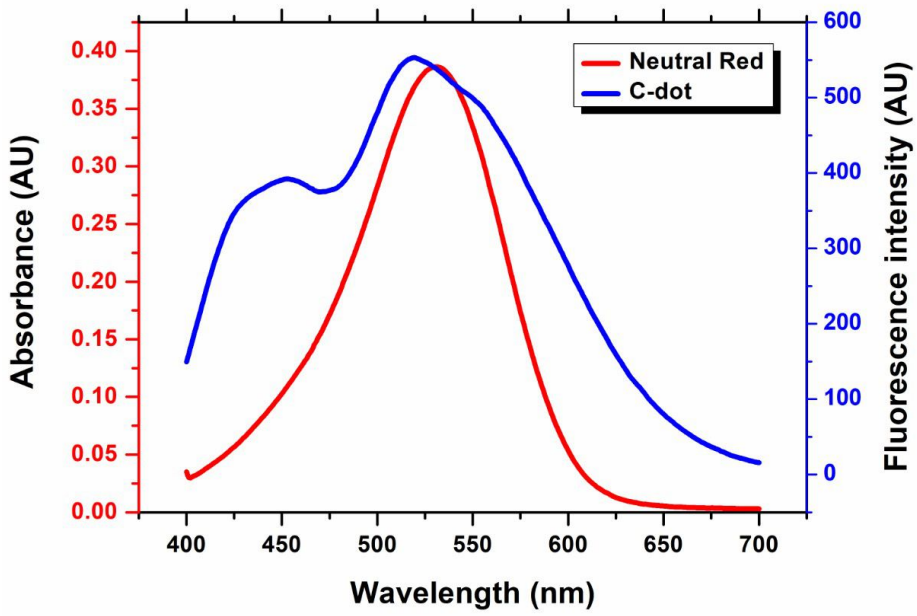

Figure 5.6: Overlapping of fluorescence spectra of the donor C-dot and absorbance spectra of the acceptor neutral red.

5.4.4 Mechanism of colorimetric and fluorescent response to nitrite

The C-dot-NR mixture shows variation in colorimetric and fluorescence mode in the presence of nitrite in the medium. The C-dot-NR sample exhibits reddish-pink under ambient light conditions and emits a greenish-yellow fluorescence signal when it is illuminated by a UV source of wavelength 375 nm. Under the natural light

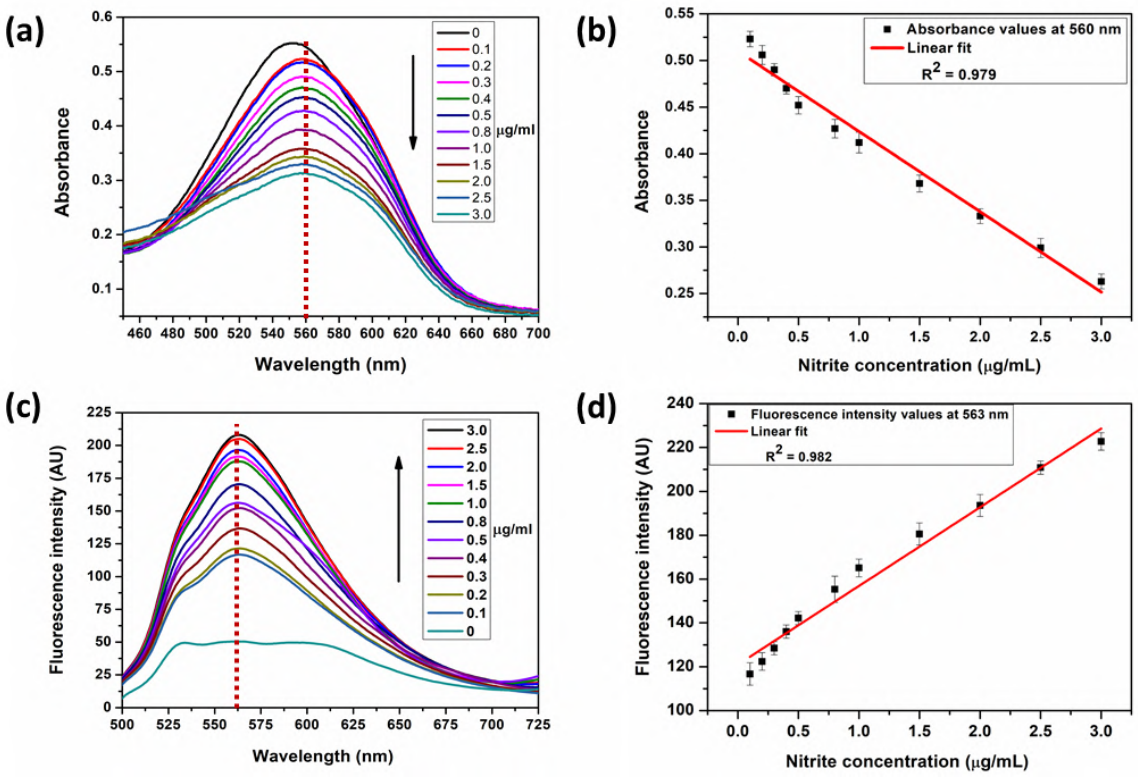

Figure 5.7: (a) Absorbance spectra and (b) calibration curve at 560 nm of the C-dot-NR samples in presence of nitrite obtained with UV-visible spectrometer (c) Fluorescence spectra and (d) calibration curve at 563 nm of the C-dot-NR samples in presence of nitrite obtained with fluorescence spectrometer.

condition, the C-dot-NR mixture changes from pink to violet with the increased nitrite concentration in the medium. The NR in the mixture acts as a chromogenic agent that gets oxidized in the presence of nitrite by forming diazonium salts and shows the colorimetric variations according to nitrite concentration present in the medium. Figure 5.7(a) shows the absorbance spectra of the C-dot-NR mixture in presence of nitrite. The absorbance of the C-dot-NR mixture decreases as the nitrite concentration increases. Figure 5.7(b) shows the characteristic graph of absorbance values at 560 nm. Again, the fluorescence emission of C-dots is recovered due to the reduction of NR in the presence of nitrite in the C-dot-NR mixture. The fluorescence intensity at the peak wavelength of 563 nm increases with the increase in nitrite concentration in the mixture. Figure 5.7(c) illustrates the characteristic fluorescence emission spectra of the C-dot-NR mixture obtained with the standard fluorescence spectrometer at different concentrations of nitrite in the medium while figure 5.7(d) represents the calibration curve for the fluorescence intensity values recorded at 563 nm.

5.5 Dual-mode detection of nitrite by the designed smartphone sensing system

5.5.1 Photometric detection

The C-dot-NR samples show colorimetric change with nitrite level concentration in the range 0.1 - 3 μg /ml. Figure 5.8(a) illustrates the photo images of the C-dot-NR samples that contained different concentrations of nitrite in the medium. Figure 5.8(b) represents the photometric sensor response of the designed tool at different concentrations of nitrite in the C-dot-NR mixture. Here, nitrite concentration in the range 0.1 - 3 μg/ml has been considered to asses the characteristics of the sensor.

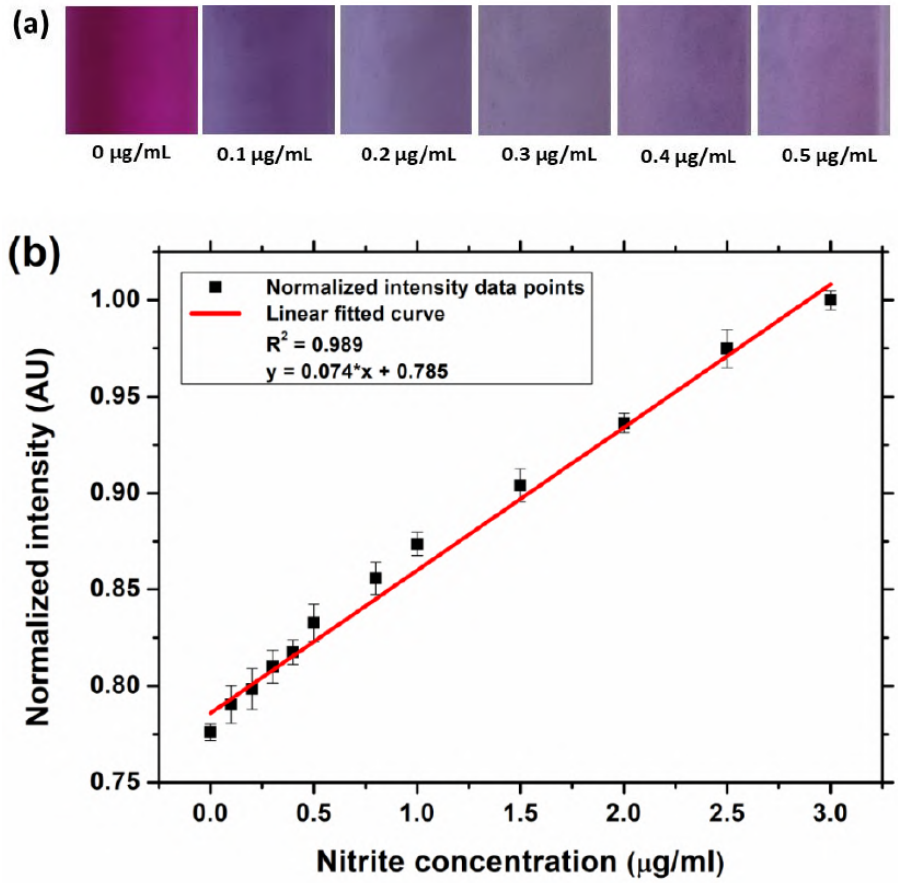

Figure 5.8: (a) Photographs of the nitrite samples showing colorimetric changes (b) Calibration curve obtained with the colorimetric-based designed sensor for the preapred samples with nitrite concentration ranging from 0.1 to 3 μg/ml.

Figure 5.8(b) depicts the characteristic curve of the sensor, which implies a linear response with regression coefficient value $R^2 = 0.989$. The error bar in the figure shows the standard deviations of the sensor response for five consecutive measurements for each sample. From the regression analysis, a calibration equation has been obtained that can be used to quantify the amount of nitrite present in a sample. The

calibration equation is given by the following equation:

$$Nitriteconcentration = \frac{Normalizedintensity - 0.78}{0.74} \tag{5.3}$$

where normalized intensity is the normalized sensor response obtained by the designed sensing tool.

5.5.2 Fluorescent detection

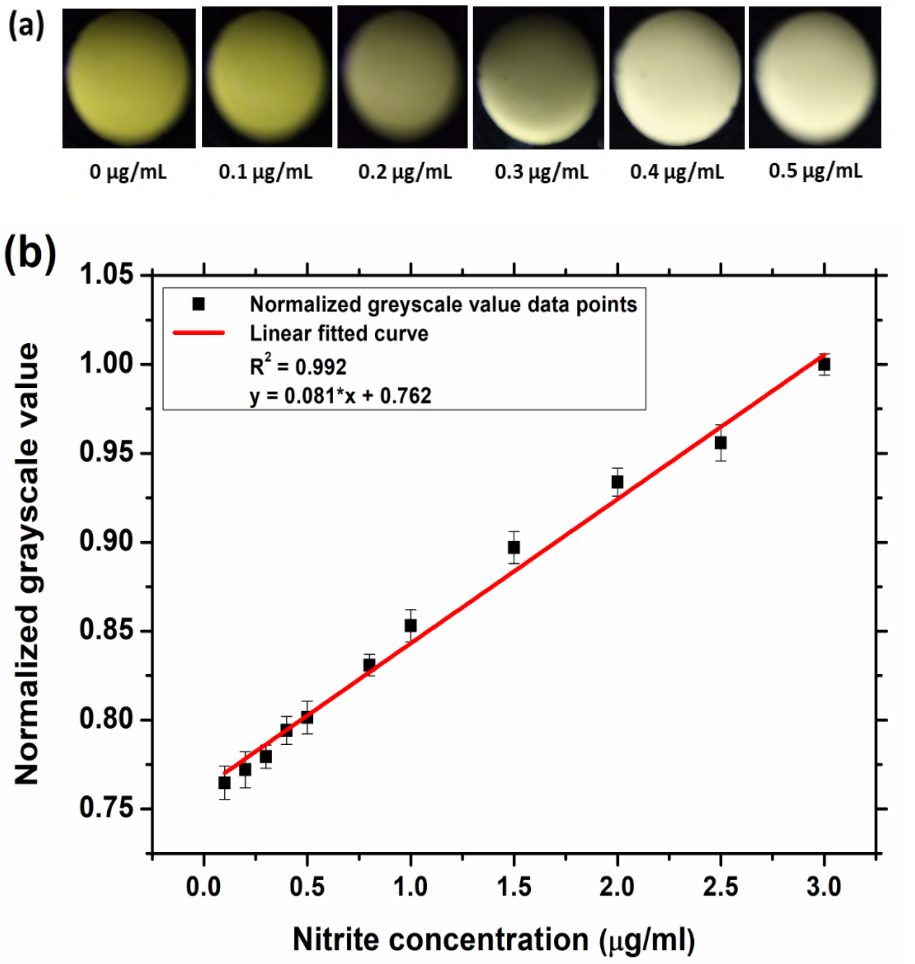

Figure 5.9: (a) Fluorescent images of the C-dot-NR nitrite samples recorded by the developed sensor (b) Calibration graph obtained with the fluorescence-based smartphone sensor for the prepared samples with nitrite concentration ranging from 0.1 to 3 μg/ml.

For fluorescence mode of detection, the emitted fluorescence signal of the C-dot-NR mixture has been acquired by the phone's imaging sensor. Figure 5.9(a) shows the photo images of the fluorescence emission signals recorded by the developed sensor for various nitrite concentrations in the medium. The characteristic fluorescence signal response at 563 nm for different concentrations of nitrite in the media is shown in

figure 5.9(b). The figure clearly indicates that with the increasing concentration of nitrite the fluorescence signal intensities increase proportionately.Figure 5.9(b) also represents the linear fitted curve of the sensor with regression coefficient $R^2 = 0.992$. The error bar in the graph depicts the standard deviations of the sensor response for five consecutive measurements of each sample. The calibration equation for the fluorescence mode of sensing can be obtained as:

$$Nitrite\ concentration = \frac{Normalized\ intensity - 0.762}{0.081} \tag{5.4}$$

From the above equation, one can easily measure the nitrite concentration of an unknown sample by incorporating the normalized greyscale value of the sample recorded by the designed sensor.

5.6 Sensor properties for both the specified sensing modalities

Table 5.1: Comparison of various sensoristic parameters in the photometric and fluorescent mode.

Sensor characteristics	**Standard equation**	**Photometric mode**	**Fluorescent mode**	**Remarks**
Sensitivity	$\frac{\Delta S}{\Delta I}$	0.05 A.U./μg/ml	0.08 A.U./μg/ml	Fluorescent sensing mode offers higher sensitivity
Limit of Detection (LoD)	$\frac{3\sigma}{S}$	0.128 μg/mL	0.116 μg/mL	Fluorescent sensing mode offers low detection limit
Accuracy (%bias)	$\frac{Known\mathrm{No_2^-} - Mean\mathrm{No_2^-}}{Known\mathrm{No_2^-}} \times 100$	0.75%	0.89%	Higher precision has been noticed in fluorescene mode of sensing
Precision (%RSD)	$\frac{Standard\ deviation}{Mean} \times 100$	2.25%	1.25%	Lower value of % RSD in the fluorescence sensing mode also signifies the higher accuracy

The sensor properties for both sensor modalities have been evaluated, and the associated sensoristic parameters in both the sensing modalities have been summarized in a tabular form (5.1). From the sensoristic parameters provided in the table 5.1, it is evident for the designed sensing platform, the fluorescence mode of sensing outperforms the photometric mode in terms of sensitivity, LoD, accuracy and precision values.

5.7 Effect of interfering elements on the sensor performance

Anti-interference performance is an important criterion to evaluate the reliability of the present sensing scheme. 1 mM solution of nine interfering elements (Cl, Br, Na, Mg, Cu, S, Mn, P and mixture of all elements) that possibly present in water and soil has been added to C-dot-NR sample mixed with 1 μg/mL standard nitrite solution. The nitrite concentrations in presence of each of the interfering elements have been estimated by the present smartphone sensor in both colorimetric and fluorescence modes and compared the results with the data obtained from a laboratory-grade spectrophotometer. Figure 5.10 depicts the bar graph illustration of the comparison

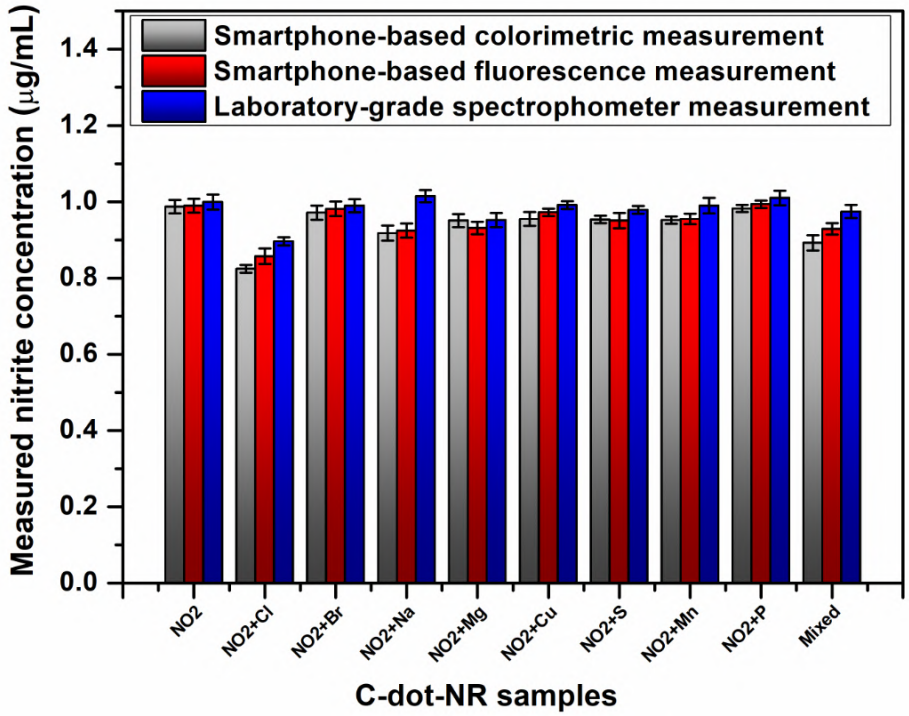

Figure 5.10: Bar graph illustration of nitrite measurements in the C-dot-NR samples mixed with nitrite in presence of considered interfering elements.

of anti-interference performance of the designed sensor with the standard tool. An

acceptably low variation of 2% in the nitrite measurement has been noticed in presence of Cl and Na in the medium. These results again suggest that the proposed sensing scheme can be reliably used to monitor nitrite content even in the presence of interfering elements in the test sample.

5.8 Sensor performance evaluations for infield samples

The performances of the developed sensing schemes for both the sensing modalities have been evaluated for infield water and soil samples. Water specimens have been acquired from ten various water sources (W1-W10) of Sonitpur district of Assam. Besides, ten soil samples (S1-S10) have been acquired from different farmlands. Prior to estimating the nitrite concentration in water, all water samples collected from different water resources have been strained with whatmann filter paper (grade 1) to extract all possible suspended particles in the sample. Similarly, following the standard protocol [48], the soil samples have been prepared in the laboratory for extraction of nitrite from the soil samples. Figure 5.11(a) and 5.11(b) illustrate the bar-graph description of the smartphone sensing data and the standard spectrometric tool for the photometric and fluorescence sensing schemes, respectively. For some of the soil samples, the experimental data error associated with the photometric sensing system is found to be higher than the standard tool attributed to the fluctuations in the sensor reading due to coupling of the high-intensity modulated signal to the ALS of the smartphone. On the other hand, the fluorescence-based smart sensing setup produces fairly comparable data to that of the conventional laboratory-grade equipment considered for this study. With the photometric mode, a maximum variation of 5% has been noticed between the experimental results obtained from the smartphone sensor and the conventional spectrophotometric tool while for the fluorescence mode of sensing, this value was found to be 3%. The relatively low variation of sensor data in the fluorescence mode suggests that this specific mode is more reliable for nitrite detection than the photometric mode of sensing. A factorial two-way ANOVA (Analysis of Variance) test [49] has been performed to compare the results obtained by the conventional spectrophotometric tool and the developed smartphone-based photometric sensor. The effect of the two tools on the results has an effect in terms of factor $F(1, 108) = 80.36$, significant value $p = 0.00$, and partial eta squared $\eta^2 = 3.93$, which suggest that there is no significant difference in the measurements recorded by the two instruments. Similarly, for the standard fluorescence spectrometer and the designed smartphone-based fluorescence sensor ANOVA test yielded a statistically significant effect, factor $F(1, 108) = 99.16$, significant value $p = 0.00$, partial eta

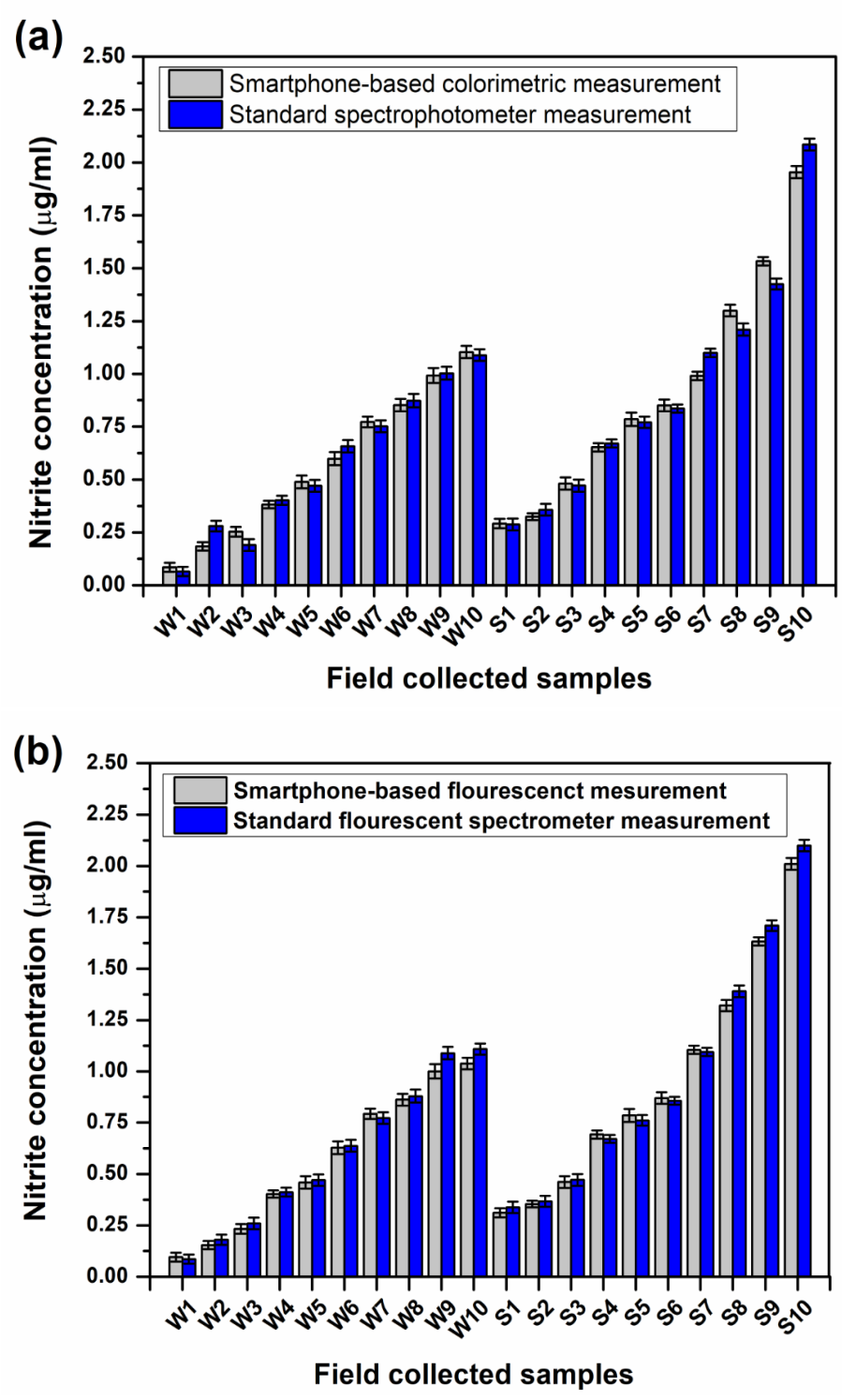

Figure 5.11: Comparative bar graph illustration of nitrite measurement by (a) the designed smartphone based photometric sensor and standard spectrophotometer and (b) the designed smartphone based fluorescent and the standard fluorescence spectrometer.

squared $\eta^2 = 4.36$, again indicating that there is no significant difference in the measurements recorded by both the tools. These experimental data clearly indicate that for nitrite concentration estimation, the designed smartphone-based sensing platform

can be used reliably in both the modalities.

5.9 Summary

In summary, the working of a dual-mode smartphone sensing system for nitrite concentration estimation in water and soil via monitoring the photometric and fluorescence signal variations from the C-dot-NR mixture has been demonstrated. The in-built ALS and CMOS image sensor have been utilized respectively, in photometric and fluorescence modes for the development of the proposed smartphone sensing system. The sensor operation in dual-mode offers a robust platform to study the nitrite concentrations on a single sensing platform. Another advantage of the dual model is that one can opt for one mode of sensing depending on the availability of the optical components. Both the sensing set-up can be coupled to the imaging sensor and the ALS of the phone as a plug-and-play tool enabling a user to choose the mode of sensing as per the requirement. The utilization of the android application makes it convenient for onboard signal and data analysis. It is envisioned that with the proposed sensing platform, various important parameters of the environment can be detected by choosing the definite protocol that shows dual-mode sensing.

References

[1] Ma, Y., Wang, Y., Xie, D., Gu, Y., Zhang, H., Wang, G., Zhang, Y., Zhao, H., and Wong, P. K. Nife-layered double hydroxide nanosheet arrays supported on carbon cloth for highly sensitive detection of nitrite. *ACS applied materials & interfaces*, 10(7):6541–6551, 2018.

[2] Wu, H. and Tong, C. Dual-emission fluorescent probe for the simultaneous detection of nitrite and mercury (ii) in environmental water samples based on the tb3+-modified carbon quantum dot/3-aminophenylboronic acid hybrid. *Analytical Chemistry*, 92(13):8859–8866, 2020.

[3] Ghanei-Motlagh, M. and Taher, M. A. A novel electrochemical sensor based on silver/halloysite nanotube/molybdenum disulfide nanocomposite for efficient nitrite sensing. *Biosensors and Bioelectronics*, 109:279–285, 2018.

[4] Adarsh, N., Shanmugasundaram, M., and Ramaiah, D. Efficient reaction based colorimetric probe for sensitive detection, quantification, and on-site analysis of nitrite ions in natural water resources. *Analytical chemistry*, 85(21):10008–10012, 2013.

[5] Baciu, A., Ardelean, M., Pop, A., Pode, R., and Manea, F. Simultaneous voltammetric/amperometric determination of sulfide and nitrite in water at bdd electrode. *Sensors*, 15(6):14526–14538, 2015.

[6] Viswanathan, P. and Ramaraj, R. Bi-functional sensing capability of gold multipod network nanostructures towards nitrite and guanine. *Sensors and Actuators B: Chemical*, 270:56–63, 2018.

[7] Titov, V. Y. and Petrenko, Y. M. Proposed mechanism of nitrite-induced methemoglobinemia. *Biochemistry (Moscow)*, 70(4):473–483, 2005.

[8] Fanning, J. C. The chemical reduction of nitrate in aqueous solution. *Coordination Chemistry Reviews*, 199(1):159–179, 2000.

[9] Li, T., Li, Y., Zhang, Y., Dong, C., Shen, Z., and Wu, A. A colorimetric nitrite detection system with excellent selectivity and high sensitivity based on ag@ au nanoparticles. *Analyst*, 140(4):1076–1081, 2015.

[10] Organization, W. H. et al. *Disinfectants and Disinfectant By-Products-Environmental Health Criteria 216*. 2000.

[11] Organization, W. H. et al. Safe drinking-water from desalination. Technical report, World Health Organization, 2011.

[12] Wang, H., Wan, N., Ma, L., Wang, Z., Cui, B., Han, W., and Chen, Y. A novel and simple spectrophotometric method for detection of nitrite in water. *Analyst*, 143(19):4555–4558, 2018.

[13] Miranda, K. M., Espey, M. G., and Wink, D. A. A rapid, simple spectrophotometric method for simultaneous detection of nitrate and nitrite. *Nitric oxide*, 5 (1):62–71, 2001.

[14] Zhang, Y., Nie, J., Wei, H., Xu, H., Wang, Q., Cong, Y., Tao, J., Chu, L., Zhou, Y., and Wu, X. Electrochemical detection of nitrite ions using ag/cu/mwnt nanoclusters electrodeposited on a glassy carbon electrode. *Sensors and Actuators B: Chemical*, 258:1107–1116, 2018.

[15] Xu, K., Chen, Q., Zhao, Y., Ge, C., Lin, S., and Liao, J. Cost-effective, wireless, and portable smartphone-based electrochemical system for on-site monitoring and spatial mapping of the nitrite contamination in water. *Sensors and Actuators B: Chemical*, 319:128221, 2020.

[16] Saraf, M., Rajak, R., and Mobin, S. M. A fascinating multitasking cu-mof/rgo hybrid for high performance supercapacitors and highly sensitive and selective electrochemical nitrite sensors. *Journal of Materials Chemistry A*, 4(42): 16432–16445, 2016.

[17] Rastogi, P. K., Ganesan, V., and Krishnamoorthi, S. A promising electrochemical sensing platform based on a silver nanoparticles decorated copolymer for sensitive nitrite determination. *Journal of Materials Chemistry A*, 2(4):933–943, 2014.

[18] Murray, E., Roche, P., Briet, M., Moore, B., Morrin, A., Diamond, D., and Paull, B. Fully automated, low-cost ion chromatography system for in-situ analysis of nitrite and nitrate in natural waters. *Talanta*, 216:120955, 2020.

[19] D'Amore, T., Di Taranto, A., Vita, V., Berardi, G., and Iammarino, M. Development and validation of an analytical method for nitrite and nitrate determination in meat products by capillary ion chromatography (cic). *Food Analytical Methods*, 12(8):1813–1822, 2019.

[20] Lopez-Moreno, C., Perez, I. V., and Urbano, A. M. Development and validation of an ionic chromatography method for the determination of nitrate, nitrite and chloride in meat. *Food chemistry*, 194:687–694, 2016.

[21] Zhang, M., Zhang, Z., Yuan, D., Feng, S., and Liu, B. An automatic gas-phase molecular absorption spectrometric system using a uv-led photodiode based detector for determination of nitrite and total nitrate. *Talanta*, 84(2):443–450, 2011.

[22] Brandao, G. C., Lima, D. C., and Ferreira, S. L. The chemical generation of no for the determination of nitrite by high-resolution continuum source molecular absorption spectrometry. *Talanta*, 98:231–235, 2012.

[23] Ianoul, A., Coleman, T., and Asher, S. A. Uv resonance raman spectroscopic detection of nitrate and nitrite in wastewater treatment processes. *Analytical chemistry*, 74(6):1458–1461, 2002.

[24] Chen, J., Pang, S., He, L., and Nugen, S. R. Highly sensitive and selective detection of nitrite ions using fe3o4@ sio2/au magnetic nanoparticles by surface-enhanced raman spectroscopy. *Biosensors and Bioelectronics*, 85:726–733, 2016.

[25] Lin, Z., Dou, X., Li, H., Ma, Y., and Lin, J.-M. Nitrite sensing based on the carbon dots-enhanced chemiluminescence from peroxynitrous acid and carbonate. *Talanta*, 132:457–462, 2015.

[26] Gill, A., Zajda, J., and Meyerhoff, M. E. Comparison of electrochemical nitric oxide detection methods with chemiluminescence for measuring nitrite concentration in food samples. *Analytica chimica acta*, 1077:167–173, 2019.

[27] Puangpila, C., Jakmunee, J., Pencharee, S., and Pensrisirikul, W. Mobile-phone-based colourimetric analysis for determining nitrite content in water. *Environmental Chemistry*, 15(7):403–410, 2018.

[28] Zhan, Y., Zeng, Y., Li, L., Luo, F., Qiu, B., Lin, Z., and Guo, L. Ratiometric fluorescent hydrogel test kit for on-spot visual detection of nitrite. *ACS sensors*, 4(5):1252–1260, 2019.

[29] Hu, X., Shi, J., Shi, Y., Zou, X., Tahir, H. E., Holmes, M., Zhang, W., Huang, X., Li, Z., and Xu, Y. A dual-mode sensor for colorimetric and fluorescent detection of nitrite in hams based on carbon dots-neutral red system. *Meat science*, 147: 127–134, 2019.

[30] Zan, M., Rao, L., Huang, H., Xie, W., Zhu, D., Li, L., Qie, X., Guo, S.-S., Zhao, X.-Z., Liu, W., et al. A strong green fluorescent nanoprobe for highly sensitive and selective detection of nitrite ions based on phosphorus and nitrogen co-doped carbon quantum dots. *Sensors and Actuators B: Chemical*, 262:555–561, 2018.

[31] Wu, H., Jiang, J., Gu, X., and Tong, C. Nitrogen and sulfur co-doped carbon quantum dots for highly selective and sensitive fluorescent detection of fe (iii) ions and l-cysteine. *Microchimica Acta*, 184(7):2291–2298, 2017.

[32] Tadesse, A., Hagos, M., RamaDevi, D., Basavaiah, K., and Belachew, N. Fluorescent-nitrogen-doped carbon quantum dots derived from citrus lemon juice: green synthesis, mercury (ii) ion sensing, and live cell imaging. *ACS omega*, 5(8):3889–3898, 2020.

[33] Lu, W., Gao, Y., Jiao, Y., Shuang, S., Li, C., and Dong, C. Carbon nano-dots as a fluorescent and colorimetric dual-readout probe for the detection of arginine and cu 2+ and its logic gate operation. *Nanoscale*, 9(32):11545–11552, 2017.

[34] Wu, X., Song, Y., Yan, X., Zhu, C., Ma, Y., Du, D., and Lin, Y. Carbon quantum dots as fluorescence resonance energy transfer sensors for organophosphate pesticides determination. *Biosensors and Bioelectronics*, 94:292–297, 2017.

[35] Liu, H., Ding, J., Zhang, K., and Ding, L. Construction of biomass carbon dots based fluorescence sensors and their applications in chemical and biological analysis. *TrAC Trends in Analytical Chemistry*, 118:315–337, 2019.

[36] Wang, R., Ruan, G., Sun, Y., Zhao, D., Yu, H., Zhang, C.-W., Li, L., and Liu, J. A full-wavelength coverage colorimetric sensor depending on polymer-carbon nanodots from blue to red for visual detection of nitrite via smartphone. *Dyes and Pigments*, 191:109383, 2021.

[37] Zhang, X.-X., Song, Y.-Z., Fang, F., and Wu, Z.-Y. Sensitive paper-based analytical device for fast colorimetric detection of nitrite with smartphone. *Analytical and bioanalytical chemistry*, 410(11):2665–2669, 2018.

[38] Li, W., Shi, Y., Hu, X., Li, Z., Huang, X., Holmes, M., Gong, Y., Shi, J., and Zou, X. Visual detection of nitrite in sausage based on a ratiometric fluorescent system. *Food Control*, 106:106704, 2019.

[39] Ricci, R. W., Ditzler, M., and Nestor, L. P. Discovering the beer-lambert law. *Journal of chemical Education*, 71(11):983, 1994.

[40] Husain, I., Choudhury, A., and Nath, P. Fiber-optic volumetric sensor based on beer-lambert principle. *IEEE Sensors Journal*, 13(9):3345–3346, 2013.

[41] Plataniotis, K. and Venetsanopoulos, A. N. *Color image processing and applications*. Springer Science & Business Media, 2000.

[42] Hakonen, A., Beves, J. E., and Strömberg, N. Digital colour tone for fluorescence sensing: a direct comparison of intensity, ratiometric and hue based quantification. *Analyst*, 139(14):3524–3527, 2014.

[43] Cantrell, K., Erenas, M., de Orbe-Payá, I., and Capitán-Vallvey, L. Use of the hue parameter of the hue, saturation, value color space as a quantitative analytical parameter for bitonal optical sensors. *Analytical chemistry*, 82(2): 531–542, 2010.

[44] Yang, Z., Li, Z., Xu, M., Ma, Y., Zhang, J., Su, Y., Gao, F., Wei, H., and Zhang, L. Controllable synthesis of fluorescent carbon dots and their detection application as nanoprobes. *Nano-Micro Letters*, 5(4):247–259, 2013.

[45] Gong, N., Wang, H., Li, S., Deng, Y., Chen, X., Ye, L., and Gu, W. Microwave-assisted polyol synthesis of gadolinium-doped green luminescent carbon dots as a bimodal nanoprobe. *Langmuir*, 30(36):10933–10939, 2014.

[46] Zhang, X., Jiang, M., Niu, N., Chen, Z., Li, S., Liu, S., and Li, J. Natural-product-derived carbon dots: from natural products to functional materials. *ChemSusChem*, 11(1):11–24, 2018.

[47] Tang, G., Du, L., and Su, X. Detection of melamine based on the fluorescence resonance energy transfer between cdte qds and rhodamine b. *Food chemistry*, 141(4):4060–4065, 2013.

[48] Dudala, S., Dubey, S. K., and Goel, S. Microfluidic soil nutrient detection system: integrating nitrite, ph, and electrical conductivity detection. *IEEE Sensors Journal*, 20(8):4504–4511, 2020.

[49] St, L., Wold, S., et al. Analysis of variance (anova). *Chemometrics and intelligent laboratory systems*, 6(4):259–272, 1989.